RSC Advances

PAPER

View Article Online
View Journal | View Issue

Cite this: *RSC Adv.*, 2025, **15**, 29142

Surface-modified polyimide on novel porous ceramic membranes for pervaporation desalination

Baiju He, †[a] Junlong Geng,†[a] Haoran Liu,[b] Yihua Li,*[ac] Tianlie Luo[c] and Changfei Gao[d]

Received 27th May 2025
Accepted 22nd July 2025

DOI: 10.1039/d5ra03719k

rsc.li/rsc-advances

Although pervaporation (PV) desalination is a promising solution to global freshwater scarcity, membranes suffer from unstable separation performance. This study utilized resource recycling to prepare a porous ceramic membrane using solid waste fly ash as raw material, which was then combined with polyimide (PI) to produce a high-performance composite membrane (abbreviated to as PI/ceramic membrane). In this composite membrane, the ceramic membrane provides mechanical support and promotes rapid water passage, while the PI layer intercepts hydrated salt ions through size screening and electronic repulsion. Through their synergistic action, the composite membrane can preferentially adsorb and diffuse water molecules while retaining. Results indicate in addition to a retention efficiency of nearly 99.9%, the PI/ceramic membranes achieved a permeability of 10.88 L (m^{-2} h^{-1}), which is superior to other existing polymer-modified membranes. Simultaneously, the membrane demonstrates selective ion rejection (*e.g.*, SO_4^{2-} and Mg^{2+}) while maintaining stable rejection performance at 90 °C. A 45-hour continuous operation test confirmed the composite membrane's stability, demonstrating consistent performance. This study provides a novel approach for the preparation of polymer-modified membranes for industrial wastewater desalination.

Introduction

In recent years, the intensifying of water supply-demand imbalances has emerged as a pressing global challenge, primarily driven by factors of population growth, climate change, and unsustainable resource management.[1,2] To address this challenge, while promoting water-saving measures, there is an urgent need to achieve water "supply expansion". Desalination technology is exactly one of the effective methods. This technology removes inorganic salts, organic matter, and impurities from seawater to produce freshwater suitable for human consumption and industrial use.[3,4] It is an effective method for addressing the current water shortage by increasing water resources. Among these, membrane separation technology has attracted extensive attention due to its high efficiency and energy-saving advantages.[5]

Among many membrane-based desalination technologies, pervaporation (abbreviated as PV) operates under ambient or low pressure conditions, offering significant energy savings compared with reverse osmosis (RO) which requires high-pressure operation, while demonstrating superior capability in treating hypersaline brines.[6] Membrane distillation (MD), a comparable membrane technology, generally imposes more stringent temperature constraints, whereas PV maintains operational stability across a wider temperature spectrum (ambient to 100 °C).[7] Consequently, membranes for PV have been deeply studied.

In general, PV membranes can be designed and synthesized from dense polymeric materials, porous inorganic materials, or hybrid matrix membranes of both.[8–10] Polyimide (abbreviate as PI) is a kind of polymer materials whose molecular main chain contains the structural features of the imide ring, with excellent thermal stability and high temperature resistance.[11,12] Due to the hydrogen bonding between its imide groups and water molecules, it has high hydrophilicity, so PI can effectively separate the target substances at high temperatures while maintaining high permeability and high selectivity. Moreover, the excellent mechanical properties of PI enable its thin film to withstand high working pressure. With further research, the combination of PI with different emerging materials has also enabled the design and preparation of membrane materials

[a]*Key Laboratory of Pollution Control Chemistry and Environmental Functional Materials for Qinghai-Tibet Plateau of the National Ethnic Affairs Commission, School of Chemistry and Environment, Southwest Minzu University, Chengdu 610041, China. E-mail: liyihua2008@163.com; yihuali@cdut.edu.cn*

[b]*Department of Chemistry, University of Liverpool, Liverpool, L69 7ZX, UK*

[c]*College of Ecology and Environment, State of Environmental Protection Key Laboratory of Synergetic Control and Joint Remediation for Soil & Water Pollution, Chengdu University of Technology, Chengdu 610059, China*

[d]*School of Environmental & Safety Engineering, Liaoning Petrochemical University, Fushun 113001, China*

† Baiju He and Junlong Geng contributed equally to this manuscript and should be considered co-first author.

with excellent properties according to specific needs.[13–15] For example, Ba *et al.*[16] used PI membrane as a carrier and prepared PMDA/ODA PI membrane through interfacial polymerization with MPDA and TMC. The membranes were used in permeation evaporation desalination tests, which achieved a 98% retention rate and a flux of 1.1 m^3 per (m^2 day) for a 2.0 g per L NaCl aqueous solution; Xu *et al.*[17] amine crosslinked PI with bis (carboxylic acid hydrazide) (BTCH) to produce pervaporation desalination composite membranes with excellent stiffness and higher hydrophilicity for desalination; Dmitrenko *et al.*[18] utilized PI and fullerenol crosslinked by a heat treatment at 140 °C for different durations (100–420 min) to form thinly crosslinked PI-fullerenol reactive layers on a porous UPM carrier for high performance of desalination. A thin crosslinked PI-fullerenol active layer was coated on UPM porous carriers to form ethanol dehydrated membranes for permeability testing; Zhang *et al.*[19] prepared PI/ATP composite membranes by *in situ* polymerization of nano-concavetite (ATP) functionalized with KH-550 silane coupling agent, which improved the gas separation performance by introducing nanoparticles into the polymer.

However, polymers are still characterized by low mechanical strength and susceptibility to swelling and aging.

Compared to conventional polymeric membrane materials, inorganic membrane materials exhibit superior chemical resistance, excellent mechanical strength, acid/alkali resistance and oxidation resistance, making them widely adopted as substrate membranes. These membranes are usually synthesized from porous inorganic materials, such as silica, alumina, and diatomaceous earth, which perform excellently in complex water treatment processes (such as radioactive-containing wastewater and high-salt waste water).[20,21] Ceramic materials have become a typical representative of inorganic membrane materials due to their outstanding characteristics, which are mainly composed of metal oxides (such as alumina, silica, and zirconia) as well as aluminosilicates.[22] The porous structure and high hydrophilicity of the ceramic membrane can not only provide mechanical support but also promote rapid water passage, while the nanoscale pores and polar groups of the separation layer can achieve preferential adsorption and diffusion of water molecules and strict interception of hydrated salt ions through size screening and electronic repulsion, respectively.[23] By modifying ceramic materials, it is possible to improve their pore size range, surface charge characteristics, *etc.* thereby broadening their application areas[24] For example, Xu *et al.*[25] prepared a high-performance polydopamine/graphene oxide composite membrane by loading a polydopamine/graphene oxide composite layer on a porous alumina ceramic substrate. The water flux of the membrane reached 8.50 L (m^{-2} h^{-1}) with a salt retention rate higher than 99.70%.

In this study, a porous ceramic-based membrane was prepared using solid waste fly ash and aluminum hydroxide, and surface modification by PI thermal cross-linking to prepare a novel PI/ceramic membrane for pervaporation desalination. The design simultaneously realizes the degree of mechanical support of the ceramic layer and the precise sieving function of the PI selective layer. Meanwhile, ceramic layer also provides the ability to assist in sieving, and the curing of the PI layer on the ceramic membrane increases its stability and reusability. And the successful modification of polyimide was confirmed by ATR-FTIR, SEM, BET, and AFM methods. The as-prepared polyimide/ceramic membranes retained sodium chloride almost completely and exhibited excellent water permeability, which was attributed to the Donnan repulsive effect on the membrane surface and the spatial site-barrier effect of the nanoscale pores.

Experimental section

Experimental materials

For specific information, see Text S1.

Preparation of porous ceramic membranes

Porous ceramic membranes were prepared with reference to our previous work.[26] In brief, fly ash (10 g), $Al(OH)_3$ (16.54 g), MoO_3 (5.31 g), and $Na_2SiO_3 \cdot 9H_2O$ (10.62 g) were mixed with 60 ml of anhydrous ethanol, wet-ground, dried, sieved, pressed into tablets, and fired to obtain the porous ceramic membrane. For more information, please see Text S3 and Fig S1.

Preparation of polyamic acid solution (PAA)

For more information, please see Text S4. The 8 wt%, 10 wt% and 12 wt% PAA solutions were prepared according to the above method for subsequent experiments.

Preparation of PI/ceramic membrane

For details of the preparation method,[27–29] please see Text S5 and Fig S2. 8 wt%, 10 wt% and 12 wt% of PAA were thermally imidized to produce composite membrane named as PI-*X*/ceramic membrane ($X = 8$, 10, 12).

Material characterization

The morphology, surface roughness, the chemical components, the zeta potential and hydrophilicity of the membranes were analyzed. The specific information, see Text S2.

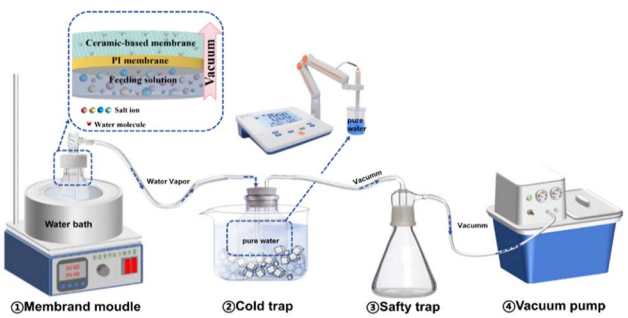

Fig. 1 Schematic diagram of the PV separation apparatus.

Desalination experiment

The experimental performance tests were evaluated by means of a homemade device made in the laboratory (Fig. 1). Explicit explanation see Text S6.

The flux and salt rejection were calculated according to eqn (1) and (2), respectively.

$$J = \frac{V}{A \cdot t} \quad (1)$$

where J (L (m^{-2} h^{-1})) is flux, V (L) denotes volume of the permeated solution collected over time t (h), and A (m^2) denotes the effective membrane area

$$R = \frac{c_f - c_P}{c_f} \times 100\% \quad (2)$$

where R (%) is rejection, C_f (mg L^{-1}) and C_p (mg L^{-1}) denotes the salt concentrations of the feed and permeated solution, respectively.

Results and discussion

Characterization

The structural evolution from PAA to PI was characterized by FTIR spectroscopy (Fig. 2 a). In the spectrum of PI, the peak at 1780 cm^{-1} attributed to asymmetric stretching vibration of carbonyl groups (C═O) in the imide ring, serving as a distinctive marker for PI formation. Additionally, the peak at 1380 cm^{-1} is the stretching vibration of the C–N bond in the imine ring, which provided conclusive evidence for the formation of PI's cyclized structure through thermoimidization. Furthermore, the peak at 729 cm^{-1} assigned to the imide ring deformation, collectively verified the complete imidization of PAA upon thermal treatment.[30–32]

The phase composition of the porous ceramic membrane was analyzed by XRD, and the result was presented in Fig. 2b. Thermal treatment induced the reaction between calcite in fly ash and corundum, forming mullite phase with a characteristic diffraction peak at 34.3°. The mullite phase exhibits characteristics of high hardness and compressive resistance, which helps to improve the overall mechanical strength and durability of the ceramic material. Simultaneously, during the sintering process at 1175 °C, both molybdenum trioxide (melting point 795 °C) present in the fly ash and calcium molybdate phase (melting point 965 °C) formed through high-temperature solid-state reaction between molybdenum trioxide and calcium oxide exhibited volatility, consequently inducing liquid-phase evolution and pore formation. This results in an intrinsically porous microstructure that facilitates water molecule transport.[33,34] Consequently, the ceramic matrix is composed of four crystalline phases: mullite, calcite, corundum, and calcium molybdate. The above distinctive multiphase structure results in membrane characteristics that with high mechanical strength and high porosity.

The pore characteristics and size distribution of both the porous ceramic membrane and PI/ceramic membrane were systematically investigated using N_2 adsorption–desorption analysis. From the results (Fig. 3a1), it can be seen that the porous ceramic membrane belongs to the type IV adsorption–desorption isothermal profile, which indicates that it is a nonporous or mesoporous material. And the relative average pore size distribution (Fig. 3a2) confirms that the porous ceramic membrane have a wide range of pore sizes ranging from mesoporous (<50 nm) to macroporous (100 nm). Complementary analysis of XRD demonstrated that the phase evolution during sintering produced mechanically robust mullite and corundum phases, while MoO_3 as a sacrificial pore-forming agent produces a heterogeneous pore structure due to its inherent thermal decomposition properties. As shown in Fig. 3b1, the PI/ceramic membrane exhibits characteristic consistent with mesoporous material, and analysis of Fig. 3b2

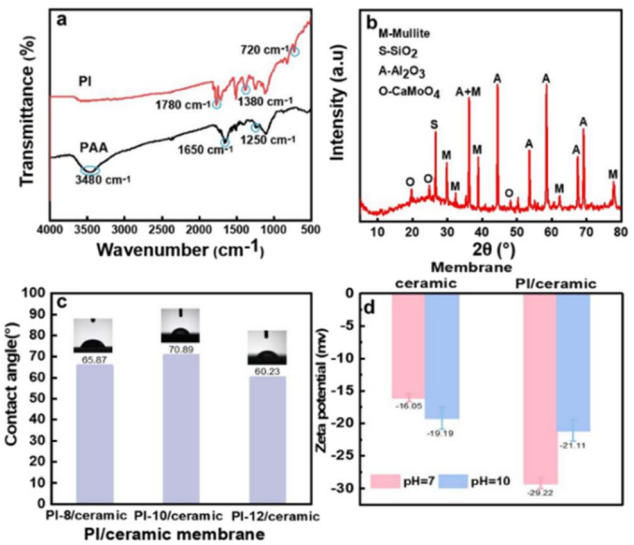

Fig. 2 Material characteristics: (a) ATR-FTIR spectra of PAA and PI, (b) XRD patterns of the porous ceramic membrane, (c) contact angles of PI-*X*/ceramic membranes, (d) zeta potentials of membrane surface.

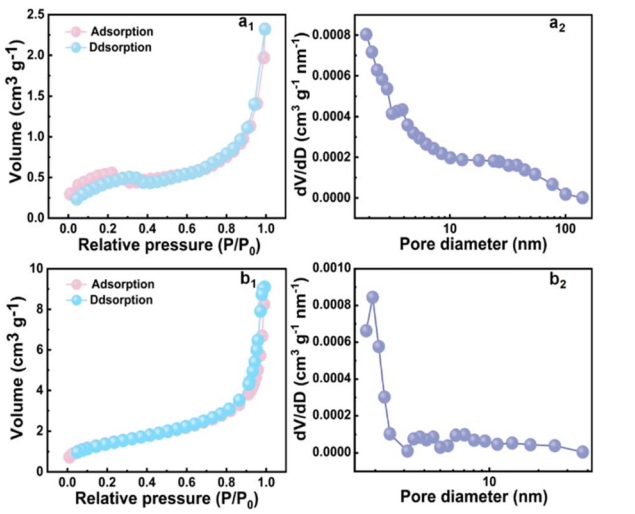

Fig. 3 N_2 adsorption and desorption isothermal curves (a1 and b1) and pore size distributions (a2 and b2) of the porous ceramic membrane (a) and PI/ceramic membrane (b).

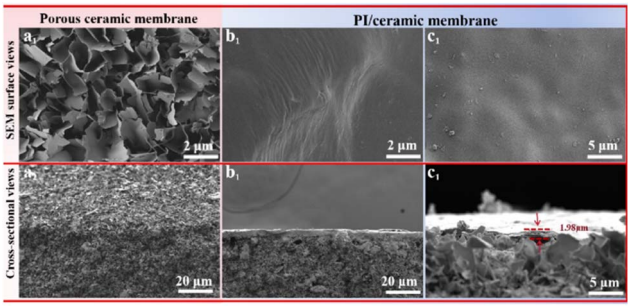

Fig. 4 SEM micrographs of (a) porous ceramic membrane of surface section (a1) and cross section (a2); PI/ceramic membrane of surface section (b1 and c1) and cross section (b2 and c2) before (b) and after (c) using.

shows that the PI/ceramic membrane are mainly distributed with pore diameters of about 10 nm, demonstrating that the PI coating effectively modulated the pore architecture of the porous ceramic membrane. Meanwhile, the comparative analysis showed that the adsorption capacity of the modified PI/ceramic membrane was larger, which meant that it had more adsorption sites, richer pore structure and larger specific surface area (Table S1). SEM analysis revealed that the porous ceramic membrane surface comprises anisotropic lamellar aggregates (Fig. 4a1). The surface irregularity provides abundant sites for PI layer deposition, facilitating effective loading and enhanced stability. The PI-modified membrane surface (Fig. 4b1) exhibits a mildly corrugated dense structure, generating microscopic bumps that enlarge the effective contact area and enhance mass transfer pathways. Cross-sectional comparison (Fig. 4a2 and b2) revealed a distinct PI thin layer post-modification, confirming successful integration of the PI layer with the porous ceramic membrane. AFM analysis further demonstrated that the porous ceramic membrane exhibited high surface roughness (R_a = 322 nm), whereas PI layer deposition significantly reduced the composite membrane roughness (R_a = 30.2 nm) (Fig. 5 and Table S1). The modulation of surface roughness exerts dual improvements on membrane performance: first by suppressing hydrodynamic perturbations to optimize filtration kinetics, and secondly by circumventing the contamination-enhancing effect induced by micron-scale depressions.

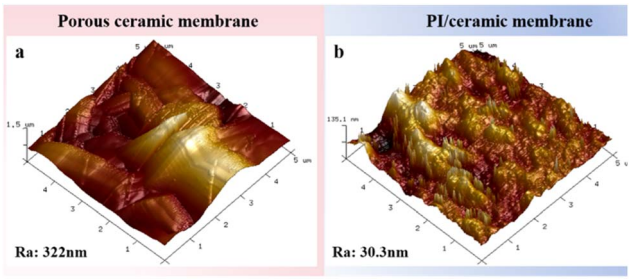

Fig. 5 AFM images of (a) porous ceramic membrane and (b) PI/ceramic membrane.

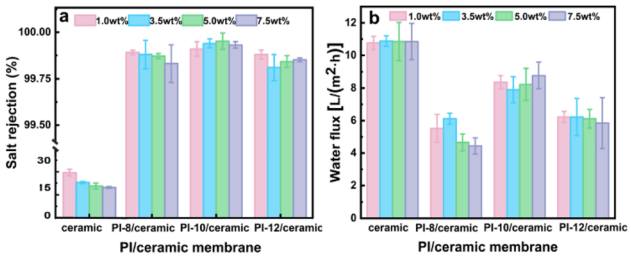

Fig. 6 Salt rejection rates and water fluxes of PI-*X*/ceramic membrane with different concentrations (a) salt rejection (b) water flux.

Desalination and permeability of different PI/ceramic membrane

In order to verify the performance of PI/ceramic membranes, we prepared PI-*X* (X = 8, 10, 12) while desalination tests were performed on simulated seawater (Fig. 6). All three membranes achieved a high rejection effect (>99%) for different concentrations of simulated seawater, which was much higher than that of the porous ceramic membrane (<30%). This confirms the effective rejection of the PI layer, and it can be seen that the PI/ceramic membrane has quality rejection ability for a wide range of salt solutions. Compared to the pure ceramic membrane (10.88 L (m^{-2} h^{-1})), PI/ceramic membranes showed different degrees of water flux decrease, which is consistent with the successful loading of the PI dense layer. The lowest decrease (about 20%) was observed for PI-10/ceramic membrane, which may be related to its moderate water affinity (Fig. 2c), which can maintain a good adsorption capacity for water molecules while reducing the retention time of water molecules on the membrane surface, thus avoiding the formation of a dense water layer.[35,36]

The temperature effect to desalination performance

The PV process is driven by the transmembrane vapor pressure gradient and the chemical potential difference, and the vapor pressure increases exponentially with temperature. Consequently, increasing the feed temperature would accelerate molecular transport and significantly increase the water flux through the membrane.[37] In this experiment, we systematically evaluated the separation performance and permeability changes of PI-10/ceramic membranes in the temperature ranged from 60 °C to 90 °C.

As evidenced in the results (Fig. 7a), the salt rejection rate of simulated seawater (3.5 wt% NaCl solution) by PI-10/ceramic membrane consistently exceeded 99% over the temperature gradient range of 60–90 °C, which is related to the sufficiently small surface pore size of the PI-modified membranes (Fig. 3). Meanwhile the increase in water flux with increasing temperature, which is consistent with the dependence of the pervaporation desalination process on vapor pressure.[38]

The feeding concentration effect to desalination performance

The filtration performance of PI/ceramic membrane was evaluated across a salinity gradient to assess their application in

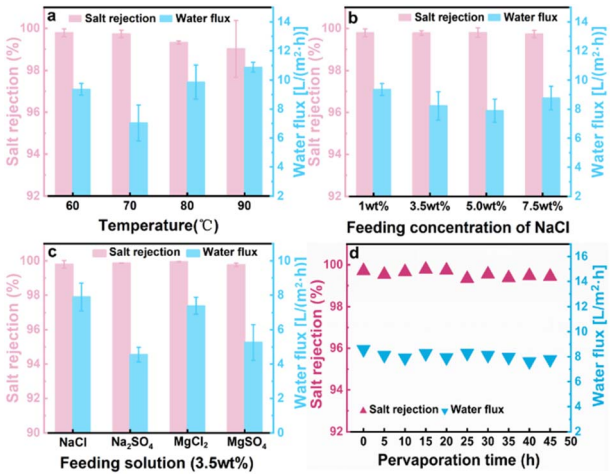

Fig. 7 Salt rejection rates and water fluxes of PI-10/ceramic membrane: (a) temperature effect (b) concentration effect (c) different salt ions (d) stability.

different water bodies such as high salinity wastewater (Fig. 7b). Remarkably, the PI-10/ceramic membrane maintained exceptional salt rejection (>99%), and the water flux was kept at a relatively stable level across the entire concentration spectrum. This is mainly attributed to the efficient retention of the PI modified layer, where the PI polymer chains are tightly aligned and sufficiently stabilized after thermoimidization. The porous ceramic membrane can also be used as a second filtration layer to provide some assistance in the retention of highly saline solutions. Despite minor flux fluctuations under high salinity conditions, the membrane retained its superior separation capability, demonstrating remarkable stability against salinity shocks.

The different ions effect to desalination performance

The PI-10/ceramic membrane was also tested in different concentrated salt solutions to make it flexible in various wastewater conditions. Therefore, different salt solutions containing SO_4^{2-}, Mg^{2+}, Na^+ and Cl^- were systematically tested. The results (Fig. 7c) showed that the PI-10/ceramic membrane had excellent separation of both monovalent and divalent ions (R > 99%). By analyzing the permeate fluxes, it can be seen that they are in the order of J (NaCl) > J ($MgCl_2$) > J ($MgSO_4$) > J (Na_2SO_4). The change in water fluxes may be due to the different hydration diameters of different salt ions, which are approximately ranked as SO_4^{2-} > Mg^{2+} > Na^+ > Cl^-.[39–41] Larger sized salt ions interact more strongly with membrane when passing through the membrane pores. The significant increase in mass-transfer resistance decreases the diffusion coefficients of the ions, thereby decreasing the permeate fluxes. Furthermore, the PI-10/ceramic membrane's negative surface potential (Fig. 2d) enhances electrostatic repulsion against anions while promoting the adsorption and deposition of cations with large hydration diameters onto the negatively charged PI layer. This selective interaction contributes to the membrane's ion rejection capability, although the adsorbed cations block the network structure and reduce water flux to some extent, this simultaneously reinforces both size-sieving and charge-repulsion mechanisms, thereby more effectively suppressing co-ion permeation.

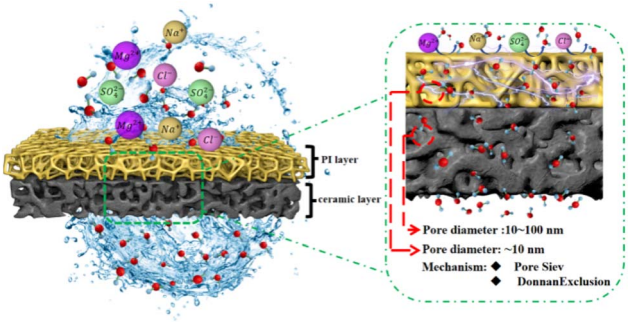

Fig. 8 Schematic diagram of water permeation through PI/ceramic membrane.

Generally, the desalination mechanisms are mainly sieving effect and Donnan effect.[42,43] In this study, the small pore size (10 nm) PI layer interacts with the interface of the mesoporous (<100 nm) ceramic layer to form a gradient structure of pore sizes from small to large from the surface to the interior, which optimizes the desalination effect. Meanwhile, the negatively charged (Fig. 2d) surface of the PI/ceramic membrane can effectively repel more of the same ions through the Donnan effect, improving the desalination efficiency. When pumping pressure pushing the side of the membrane, water can easily through the hydrophilic PI/ceramic membrane while salt ions experience combined rejection from both steric and electrostatic barriers[44] (Fig. 8).

Comparison of similar membranes and membrane stability

Compared with analogous polymer membranes (Fig. 9),[45–51] our PI-10/ceramic membranes demonstrate superior performance in the synergistic optimization of desalination efficiency and water flux. When the desalination efficiency of >99.9%, the PI-

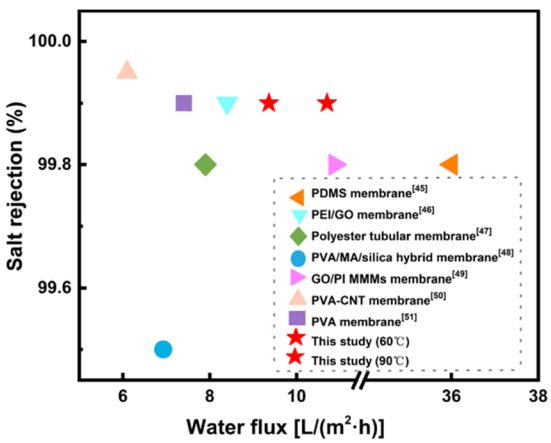

Fig. 9 Salt rejection rates and water fluxes of different polymers membranes for PV desalination.

10/ceramic membrane achieved the highest water flux (10.88 L (m^{-2} h^{-1})); when the water flux of >10 L (m^{-2} h^{-1}), the PI-10/ceramic membrane achieves optimal desalination performance.

An experiment with 45 hours of long-term desalination process by PI-10/ceramic membrane was operated. The results (Fig. 7d) showed that the PI-10/ceramic membrane almost maintained the desalination efficiency of above 99%, although the water fluxes slightly decreased, however, the fluctuation trend was not obvious. This indicates that the PI-10/ceramic membrane had a good stability. The SEM results of the PI-10/ceramic composite membranes after use showed (Fig. 4c) that little change was seen on the surface of PI-10/ceramic membrane, indicating a stable membrane surface structure after long-term operation. This further evidence that PI-10/ceramic membrane have excellent stability during long-term operation.

Conclusions

In this study, porous the PI-10/ceramic membranes were successfully developed by surface modification with PI thermal cross-linking. The modification has greatly improve both the surface roughness and the pore size range of the PI/ceramic membranes, which resulted in good desalination efficiency, high water permeability, and good stability. This study provides a new idea in the combination of polymer membranes with inorganic ceramic membranes, which shows great potential in the treatment of industrial wastewater desalination.

Author contributions

Baiju He: formal analysis, writing – original draft. Junlong Geng: methodology, validation. Haoran Liu: methodology, figure supplementation and test polishing; Yihua Li: conceptualization, writing – review & editing. Tianlie Luo: visualization, supervision. Changfei Gao: investigation.

Conflicts of interest

The authors declare that they have no known competing financial interests or personal relationships that could have appeared to influence the work reported in this paper.

Data availability

All data generated or analysed during this study are included in this published article [and its SI files].

Supplementary information is available. See DOI: https://doi.org/10.1039/d5ra03719k.

Acknowledgements

This paper was funded by the National Natural Science Foundation of China (No. 42107090) and Scientific and Technological Innovation Team for Qinghai-Tibetan Plateau Research of Southwest Minzu University (No. 2024CXTD07). The authors thank Shiyanjia Lab (https://www.shiyanjia.com) for the BET, AFM and SEM analysis.

References

1 R. Z. Harifidy, I. Hiroshi, R. Z. M. Harivelo, M. G. M. Jun, S. Kazuyoshi and M. Keiichi, *Water Res.*, 2024, **257**, 121711.
2 S. H. Abebe, H. F. M. Austria, T. M. Subrahmanya, H. C. Chang, T. H. Huang, G. Carballo, W. S. Hung, C. C. Hu, K. R. Lee and J. Y. Lai, *Chem. Eng. J.*, 2025, **505**, 159644.
3 M. Yi, Q. Xia, J. L. Tan, J. W. Shang and X. W. Cheng, *Chem. Eng. J.*, 2024, **493**, 152568.
4 K. Harby, M. Emad, M. Benghanem, T. Z. Abolibda, K. Almohammadi, A. Aljabri, A. Alsaiari and M. Elgendi, *Desalination*, 2024, **581**, 117600.
5 M. Fu, C. H. Chen, S. Zhang, Y. H. You, H. F. Zhao, B. Lin, S. Q. Wang and Y. C. Dong, *Chem. Eng. J.*, 2024, **502**, 157949.
6 C. Q. Cao, F. N. Liu, F. Q. Li, O. R. Uzochukwu and L. Chen, *Desalination*, 2024, **574**, 117263.
7 G. Yang, Z. L. Xie, M. Cran, C. R. Wu and S. Gray, *Membranes*, 2020, **10**, 10090193.
8 E. Bakangura, L. Wu, L. Ge, Z. J. Yang and T. W. Xu, *Prog. Polym. Sci.*, 2016, **57**, 103–152.
9 S. Karki, G. Hazarika, D. Yadav and P. G. Ingole, *Desalination*, 2024, **573**, 117200.
10 A. Saravanan, P. Thamarai, P. S. Kumar and G. Rangasamy, *Chemosphere*, 2022, **308**, 136318.
11 Y. H. Li, G. H. Sun, Y. Zhou, G. M. Liu, J. Wang and S. H. Han, *Prog. Org. Coat.*, 2022, **172**, 107103.
12 B. Y. Zou, S. Zhao, F. Bao, L. Zhou, B. X. He, Y. Zhao, J. S. Zhang, W. F. Peng, Y. Shen, M. J. Huang and C. W. Nan, *Adv. Funct. Mater.*, 2025, 2505254.
13 T. T. Xue, C. Y. Zhu, D. Y. Yu, X. Zhang, F. L. Lai, L. S. Zhang, C. Zhang, W. Fan and T. X. Liu, *Nat. Commun.*, 2023, **14**, 8378.
14 Y. Li, B. Ma, R. B. Zhang and X. G. Luo, *Polymer*, 2022, **253**, 125035.
15 M. C. Wang, J. Y. Liao, C. Y. Gao, J. W. Ma, X. J. Meng, Y. H. Shen, X. Wu, Y. Wang and J. P. Li, *J. Membr. Sci.*, 2025, **720**, 123713.
16 C. Y. Ba and J. Economy, *J. Membr. Sci.*, 2010, **363**, 140–148.
17 S. Xu, L. F. Liu and Y. Wang, *Sep. Purif. Technol.*, 2017, **185**, 215–226.
18 M. E. Dmitrenko, A. V. Penkova, A. B. Missyul, A. I. Kuzminova, D. A. Markelov, S. S. Ermakov and D. Roizard, *Sep. Purif. Technol.*, 2017, **187**, 285–293.
19 S. Y. Zhang, X. C. Lu, M. W. Cai, Z. Wang, Z. J. Han, Z. Y. Chen, R. T. Liu, K. X. Li and Y. G. Min, *Polymers*, 2022, **14**, 54.
20 B. B. Liu, Z. G. Wang and X. Y. Tan, *J. Membr. Sci.*, 2025, **726**, 123983.
21 E. L. Zhang, L. L. Liu, S. W. Jin, P. H. Zhao, X. Z. Wang and G. G. Xu, *Ceram. Int.*, 2025, **51**, 15512–15520.
22 D. Zou, Z. X. Zhong and Y. Q. Fan, *Sep. Purif. Technol.*, 2024, **338**, 126441.

23 L. Zhou, H. Yu, M. Y. Hossain, F. Chen, C. H. Du and G. Q. Zhang, *Chem. Eng. J.*, 2023, **470**, 145180.
24 P. Innocenzi and L. Malfatti, *J. Photochem. Photobiol., C*, 2024, **58**, 100652.
25 K. Xu, B. Feng, C. Zhou and A. S. Huang, *Chem. Eng. Sci.*, 2016, **146**, 159–165.
26 J. Jiao, Y. H. Li, T. L. Luo, Q. Song, L. F. Liu and B. C. Liu, *Separ. Purif. Technol.*, 2023, **323**, 124415.
27 N. N. Song, T. N. Ma, T. J. Wang, Z. H. Li, H. Y. Yao and S. W. Guan, *J. Colloid Interface Sci.*, 2020, **573**, 328–335.
28 M. Fu, J. Liu, X. F. Dong, L. Zhu, Y. C. Dong and S. Hampshire, *J. Eur. Ceram. Soc.*, 2019, **39**, 5320–5331.
29 Y. Zhang, Y. J. Wu, X. K. Yang, D. H. Li, X. Y. Zhang, X. Dong, X. H. Yao, J. C. Liu and A. R. Guo, *J. Eur. Ceram. Soc.*, 2020, **40**, 2090–2096.
30 K. C. Chang, K. Y. Huang, C. H. Hsu, W. F. Ji, M. C. Lai, W. I. Hung, T. L. Chuang and J. M. Yeh, *Eur. Polym. J.*, 2014, **56**, 26–32.
31 A. Abdullaev, X. Y. Mei, F. J. Liu, K. Peng, Y. J. You, F. Y. Wu, M. Z. Islam, Q. B. Yang, Y. S. Si and Y. Q. Fu, *ACS Appl. Mater. Interfaces*, 2024, **16**, 61004–61015.
32 J. H. Xin, X. W. Zhou, G. L. Huo, Z. G. Zhang, Y. C. Zhang, S. Y. Kang, Z. D. Dai and N. W. Li, *J. Membr. Sci.*, 2023, **688**, 122123.
33 Y. Chen, N. N. Wang, O. Ola, Y. D. Xia and Y. Q. Zhu, *Mater. Sci. Eng. R Rep.*, 2021, **143**, 100589.
34 Q. S. Wu, Q. J. Chen, Z. C. Huang, B. Gu, H. J. Zhu and L. Tian, *Ceram. Int.*, 2020, **46**, 4581–4586.
35 S. Kim, J. Hou, N. R. Choudhury and S. E. Kentish, *Energy Environ. Mater.*, 2025, **8**, e12841.
36 Y. Z. Yan, K. Chen, H. Moon, S. S. Park and C. S. Ha, *Eur. Polym. J.*, 2024, **202**, 112633.
37 K. Kawajiri, T. Oozeki and Y. Genchi, *Environ. Sci. Technol.*, 2011, **45**, 9030–9035.
38 J. Q. Pu, H. Y. Zhu, Q. Wang, Z. G. Qu and J. F. Zhang, *ACS Energy Lett.*, 2024, **9**, 2410–2419.
39 D. Beyer and C. Holm, *ACS Macro Lett.*, 2024, 1185–1191.
40 F. Wang and V. V. Tarabara, *J. Membr. Sci.*, 2007, **293**, 111–123.
41 Z. H. Wang, J. W. Sun, N. Li, Y. Z. Qin, X. W. Qian and Z. L. Xie, *Sep. Purif. Technol.*, 2022, **286**, 120458.
42 H. Wang, R. Ding, T. Wu, X. J. Zhang, L. J. Cheng, K. Xu, Y. Zheng, X. Pang, G. L. Ji, L. Q. Shen, J. J. Li, R. N. Zhang and Z. Y. Jiang, *Chem. Eng. J.*, 2025, **510**, 161593.
43 W. Zhao, H. Gong, Y. Song, B. Li, N. Xu, X. Z. Min, G. L. Liu, B. Zhu, L. Zhou, X. X. Zhang and J. Zhu, *Adv. Funct. Mater.*, 2021, **31**, 52.
44 L. Cumbal and A. K. SenGupta, *Environ. Sci. Technol.*, 2005, **39**, 6508–6515.
45 G. Genduso, A. Missinne, Z. Ali, W. Ogieglo, B. Van der Bruggen and I. Pinnau, *Sep. Purif. Technol.*, 2022, **280**, 119819.
46 E. Halakoo and X. S. Feng, *Sep. Purif. Technol.*, 2020, **234**, 116077.
47 M. N. Sule, M. R. Templeton and T. Bond, *Environ. Technol.*, 2016, **37**, 1382–1389.
48 Z. Xie, M. Hoang, T. Duong, D. Ng, B. Dao and S. Gray, *J. Membr. Sci.*, 2011, **383**, 96–103.
49 B. Feng, K. Xu and A. S. Huang, *RSC Adv.*, 2017, **7**, 2211–2217.
50 C. Tseng and Y. L. Liu, *J. Membr. Sci.*, 2023, **668**, 121185.
51 S. G. Chaudhri, B. H. Rajai and P. S. Singh, *Desalination*, 2015, **367**, 272–284.